ПН
780/525

Volume 213 May 2014 ISSN 0022-4596

ELSEVIER

JOURNAL OF SOLID STATE CHEMISTRY

Editor
M.G. KANATZIDIS

Associate Editors
S.J. HWANG
J. LI
S.J. CLARKE
H.-C. ZUR LOYE

IN THIS ISSUE:

Mixed ligand coordination polymers with flexible bis-imidazole linker and angular sulfonyldibenzoate: Crystal structure, photoluminescence and photocatalytic activity

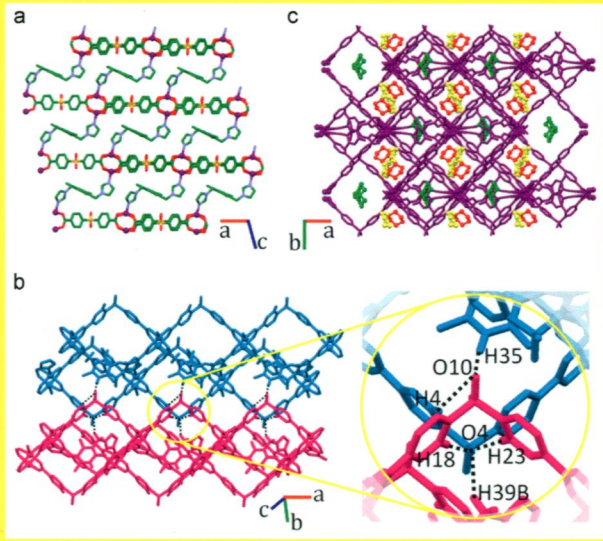

Kamal Kumar Bisht, Yadagiri Rachuri, Bhavesh Parmar and Eringathodi Suresh

Available online at www.sciencedirect.com

ScienceDirect

ELSEVIER

Volume 213, May 2014

CONTENTS

JOURNAL OF SOLID STATE CHEMISTRY

www.elsevier.com/locate/jssc

Abstracted/indexed in BioEngineering Abstracts, Chemical Abstracts, Coal Abstracts, Current Contents/Physics, Chemical, & Earth Sciences, Engineering Index, Research Alert, SCISEARCH, Science Abstracts, and Science Citation Index. Also covered in the abstract and citation database SCOPUS®. Full text available on ScienceDirect®.

Regular Articles

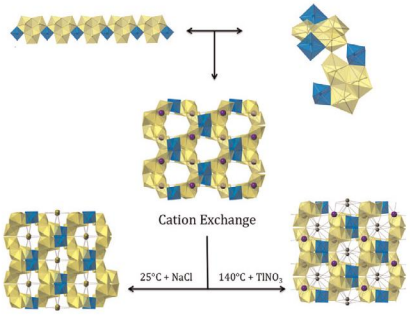

Chains of uranium and tungsten polyhedra are connected into a three dimensional framework by cation–cation interactions occurring between two symmetrically independent uranyl pentagonal bipyramids. Monovalent cations present in channels within the structure can be exchanged by room temperature or mild hydrothermal treatments. The framework of these compounds is robust to cation exchange and heat. (yellow polyhedra = uranium pentagonal bipyramids; blue polyhedra = tungsten octahedral, purple balls = K; yellow balls = Na; grey balls = Tl)

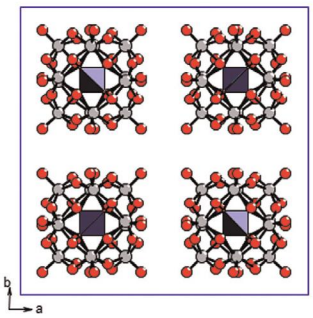

Relative arrangements of HPA clusters in $(K_5, H_3O)[SiV_3W_9O_{40}]\cdot xH_2O$.

Regular Articles—Continued

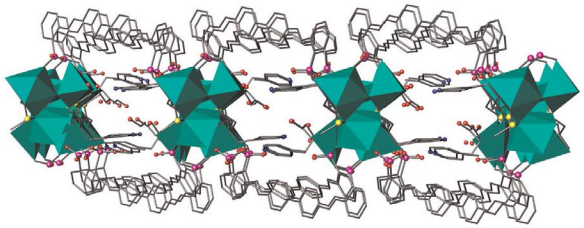

A new lead sulfonate with sandwich-like 2D hybrid layer consisting of hexanuclear lead clusters and 1D channels.

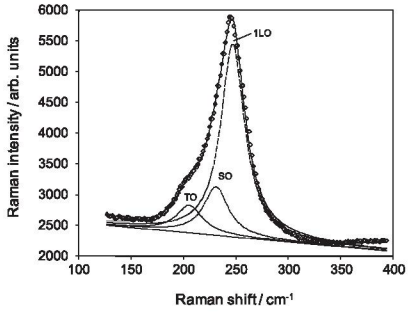

Optical phonons in nanostructured thin films composed by zincblende zinc selenide quantum dots in strong size-quantization regime: competition between phonon confinement and strain-related effects.

Continued

The analysis of magnesium oxide hydration in three-phase reaction system

Xiaojia Tang, Lin Guo, Chen Chen, Quan Liu, Tie Li and Yimin Zhu

page 32

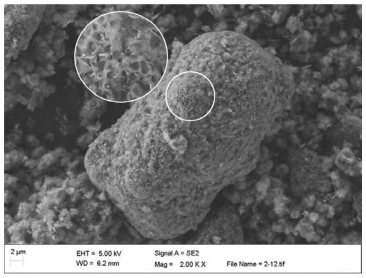

There was existence of a peeling-off process in the gas–liquid–solid (three-phase) MgO hydration system.

History-dependent thermal expansion in NbO_2F

Angus P. Wilkinson, Ryan E. Josefsberg, Leighanne C. Gallington, Cody R. Morelock and Christopher M. Monaco

page 38

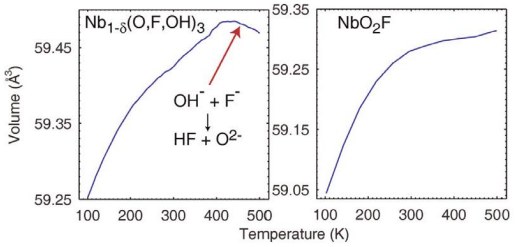

"NbO_2F" prepared by the digestion of Nb_2O_5 in HF contains cation vacancies and hydroxyl groups. It undergoes irreversible changes on heating to low temperatures, unlike NbO_2F prepared by the solid state reaction of Nb_2O_5 and NbF_5

Mixed ligand coordination polymers with flexible bis-imidazole linker and angular sulfonyldibenzoate: Crystal structure, photoluminescence and photocatalytic activity

Kamal Kumar Bisht, Yadagiri Rachuri, Bhavesh Parmar and Eringathodi Suresh

page 43

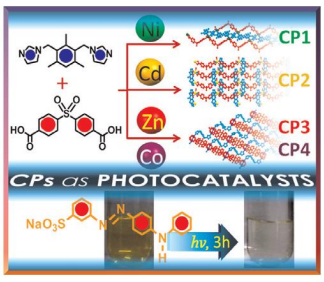

Four new ternary transition metal CPs have been hydrothermally prepared and their structural aspects as well as photocatalytic activity for decolourization of metanil yellow (MY) dye have been investigated.

Crystallite-growth, phase transition, magnetic properties, and sintering behaviour of nano-$CuFe_2O_4$ powders prepared by a combustion-like process

Roberto Köferstein, Till Walther, Dietrich Hesse and Stefan G. Ebbinghaus

page 57

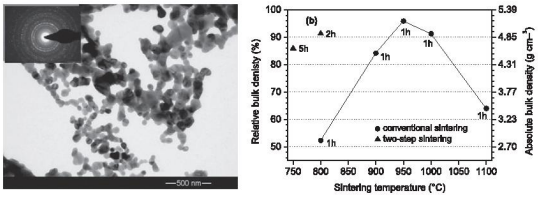

A cheap one-pot synthesis was developed to obtain $CuFe_2O_4$ nano-powders with different crystallite sizes (36–96 nm). The optical band gaps, phase transition temperatures and enthalpies were determined depending on the particle size. The sintering behaviour of nano $CuFe_2O_4$ was studied in different sintering procedures. The magnetic behaviour of the nano-powders as well as the corresponding ceramic bodies were investigated.

Structure and photoluminescence properties of $Na_2Y_2B_2O_7:Ce^{3+},Tb^{3+}$ phosphors for solid-state lighting application

Dawei Wen, Hui Yang, Guanhui Yang, Jianxin Shi, Mingmei Wu and Qiang Su

page 65

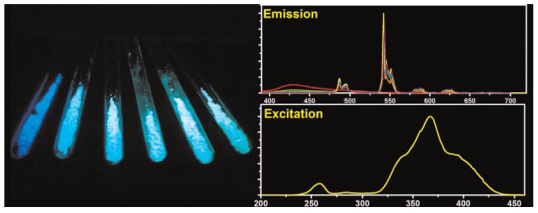

Colour-tunable phosphors $Na_2Y_2B_2O_7:Ce^{3+},Tb^{3+}$ with optimal quantum yield of 75.2% are synthesized and the phosphors can be served as *n*-UV pumped materials for LEDs.

Electrical properties of $(1-x)(Bi_{0.5}Na_{0.5})TiO_3$–$xKNbO_3$ lead-free ceramics

Xijie Jiang, Baoyin Wang, Laihui Luo, Weiping Li, Jun Zhou and Hongbing Chen

page 72

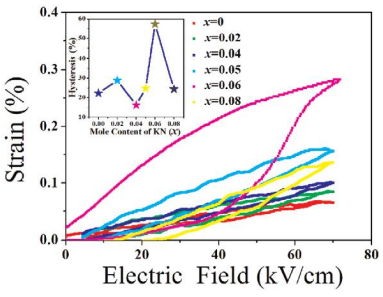

Unipolar electric-field-induced strain for the BNT–*x*KN ceramics. A maximum strain of 0.28% is achieved with a low field in BNT–0.06KN.

VO_2 (A): Reinvestigation of crystal structure, phase transition and crystal growth mechanisms
Srinivasa Rao Popuri, Alla Artemenko, Christine Labrugere, Marinela Miclau, Antoine Villesuzanne and Michaël Pollet
page 79

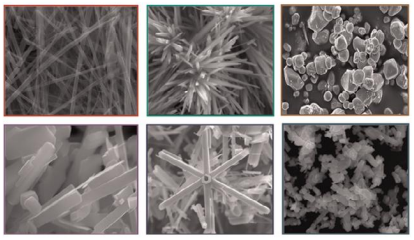

Using a single step and template free hydrothermal synthesis, well crystallized VO_2 (A) microrods were prepared and the *P4/ncc* space group was assigned to the room temperature crystal structure. Reversible and irreversible phase transitions among different VO_2 polymorphs were identified and their progressive nature was highlighted. Attempts to increase the microrods size, involving layer by layer formation mechanisms, are presented.

Rare-earth transition-metal chalcogenides Ln_3MGaS_7 (*Ln*=Nd, Sm, Dy, Er; *M*=Co, Ni) and Ln_3MGaSe_7 (*Ln*=Nd, Sm, Gd, Dy, *M*=Co; *Ln*=Nd, Gd, Dy, *M*=Ni)
Wenlong Yin, Youguo Shi, Bin Kang, Jianguo Deng, Jiyong Yao and Yicheng Wu
page 87

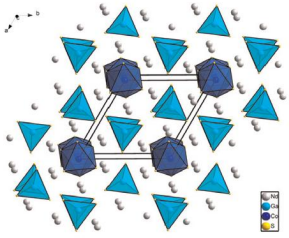

Ln_3MGaS_7 (*Ln*=Nd, Sm, Dy, Er; *M*=Co, Ni) and Ln_3MGaSe_7 (*Ln*=Nd, Sm, Gd, Dy, *M*=Co; *Ln*=Nd, Gd, Dy, *M*=Ni) adopt a three-dimensional framework composed of LnQ_7 monocapped trigonal prisms with interesting $[MQ_3]^{4-}$ chains and isolated GaQ_4 tetrahedra lying in two sets of channels in the framework.

The impact of oxygen nonstoichiometry upon partial molar thermodynamic quantities in $PrBaCo_2O_{5+\delta}$
A.Yu. Suntsov, I.A. Leonidov, M.V. Patrakeev and V.L. Kozhevnikov
page 93

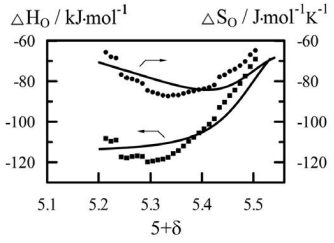

Partial thermodynamic functions of movable oxygen in $PrBaCo_2O_{5+\delta}$.

Morphology-controlled synthesis of Ti^{3+} self-doped yolk–shell structure titanium oxide with superior photocatalytic activity under visible light
Shixiong Wang, Xiangjun Yang, Yapeng Wang, Lixiang Liu, Yuanyuan Guo and Hong Guo
page 98

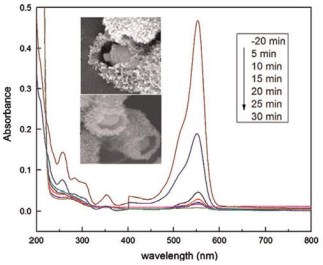

A facile generic strategy is employed to prepare Ti^{3+} self-doped yolk–shell structure titanium oxide nanoparticle aggregates with the superior photocatalytic activity under visible light.

Fe_3O_4–CNTs nanocomposites: Inorganic dispersant assisted hydrothermal synthesis and application in lithium ion batteries
Qixun Guo, Pengfei Guo, Juntao Li, Hao Yin, Jie Liu, Feilong Xiao, Daoxiang Shen and Ning Li
page 104

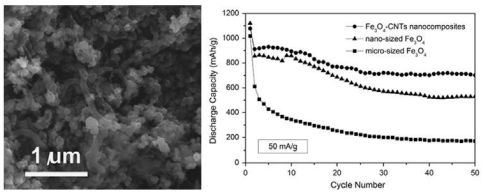

Fe_3O_4–CNTs nanocomposites have been prepared through an inorganic dispersant assisted hydrothermal synthesis strategy, and served as anode materials of lithium ion batteries with enhanced performance.

High-pressure U_3O_8 with the fluorite-type structure
F.X. Zhang, M. Lang, J.W. Wang, W.X. Li, K. Sun, V. Prakapenka and R.C. Ewing
page 110

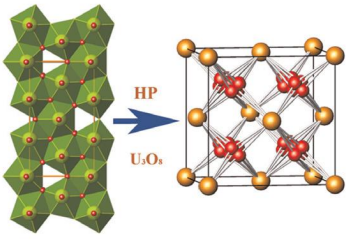

α-U_3O_8 is in a layered structure with orthorhombic symmetry, at high pressures, it transformed to a fluorite-type cubic structure. There are a lot of defects in the cubic structure, and it is a new kind of hyperstoichiometric uranium oxide, which is stable at ambient conditions.

Continued

The electronic structure of the antimony chalcogenide series: Prospects for optoelectronic applications

John J. Carey, Jeremy P. Allen, David O. Scanlon and Graeme W. Watson

page 116

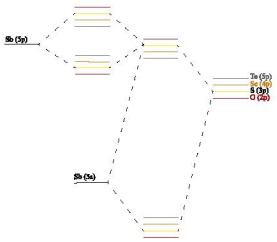

A schematic illustrating the interaction between the Sb^{III} cations and the chalcogenide anions and the change in their respective energy levels down the series.

Optical properties of Eu^{2+}/Eu^{3+} mixed valence, silicon nitride based materials

Otmar M. ten Kate, Thomas Vranken, Erik van der Kolk, Antonius P.J. Jansen and Hubertus T. Hintzen

page 126

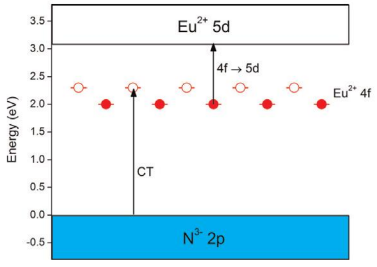

Energy level scheme of Eu_2SiN_3 showing the occupied N^{3-} 2*p* band (blue rectangle), unoccupied Eu^{2+} 5*d* band (white rectangle), occupied Eu^{2+} 4*f* ground states (filled red circles) and unoccupied Eu^{2+} ground states (open red circles).

Investigation into the effect of Si doping on the cell symmetry and performance of $Sr_{1-y}Ca_yFeO_{3-\delta}$ SOFC cathode materials

Jose M. Porras-Vazquez, R.I. Smith and Peter R. Slater

page 132

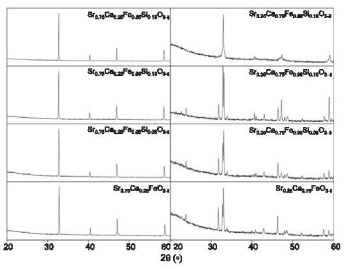

X-ray diffraction patterns for: (left) $Sr_{0.75}Ca_{0.25}Fe_{1-x}Si_xO_{3-\delta}$ (x=0, 0.05, 0.10 and 0.15) and (right) $Sr_{0.25}Ca_{0.75}Fe_{1-x}Si_xO_{3-\delta}$ (x=0, 0.05, 0.10 and 0.15), showing the stabilization of the cubic form of these series through silicon doping. For the latter $Sr_{0.25}Ca_{0.75}Fe_{1-x}Si_xO_{3-\delta}$ phase, the stabilisation is not quite complete at 15% Si doping.

Comparative study of A-site order in the lead-free bismuth titanates $M_{1/2}Bi_{1/2}TiO_3$ (M=Li, Na, K, Rb, Cs, Ag, Tl) from first-principles

Melanie Gröting and Karsten Albe

page 138

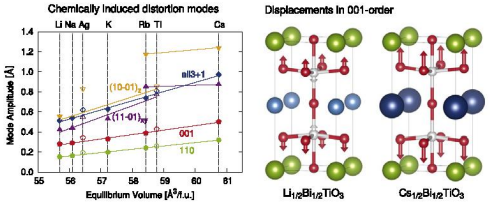

Amplitudes of chemically induced distortion modes in different ordered perovskites $M_{1/2}Bi_{1/2}TiO_3$ and visualisation of atomic displacements associated with distortion mode X_1^+ in the 001-ordered compounds $Li_{1/2}Bi_{1/2}TiO_3$ and $Cs_{1/2}Bi_{1/2}TiO_3$. Due to a substantial size mismatch between bismuth (green) and caesium (dark blue), incorporation of the latter leads to enhanced displacements of oxygen atoms (red) and suppresses displacements of titanium (silver) as compared to lithium (light blue) or other smaller monovalent cations.

The role of SO_4^{2-} surface distribution in arsenic removal by iron oxy-hydroxides

S. Tresintsi, K. Simeonidis, N. Pliatsikas, G. Vourlias, P. Patsalas and M. Mitrakas

page 145

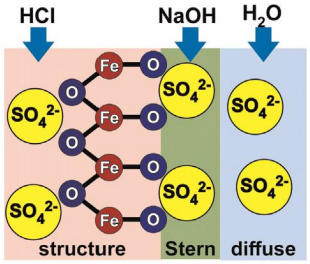

An analytical methodology for the accurate quantification of sulfate ions (SO_4^{2-}) distribution onto the diffuse layer, the Stern layer and the structure of iron oxy-hydroxides used as arsenic removal agents.

The Li–Si–(O)–N system revisited: Structural characterization of $Li_{21}Si_3N_{11}$ and Li_7SiN_3O

M. Casas-Cabanas, H. Santner and M.R. Palacín

page 152

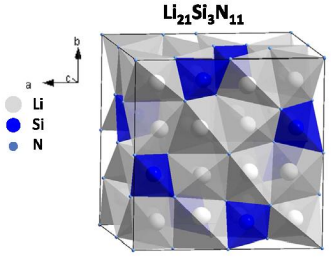

A systematic study of the Li–Si–(O)–N system is presented. $Li_{21}Si_3N_{11}$ crystallizes as a superstructure of the anti-fluorite structure with Li and Si ordering, Li_7SiN_3O exhibits the anti-fluorite structure with both anion and cation disorder.

Synthesis of finely divided molybdenum sulfide nanoparticles in propylene carbonate solution
Pavel Afanasiev
page 158

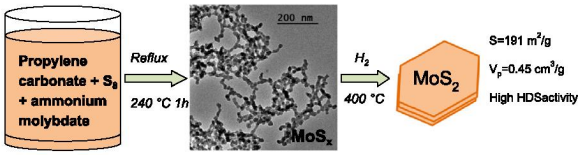

Solution reaction in propylene carbonate allows preparing weakly agglomerated molybdenum sulfide with particle size 20 nm and advantageous catalytic properties.

Crystal structure of $Mn_2Ln_3Sb_3O_{14}$ (Ln=La, Pr and Nd): A new ordered rhombohedral pyrochlore
W.T. Fu and D.J.W. IJdo
page 165

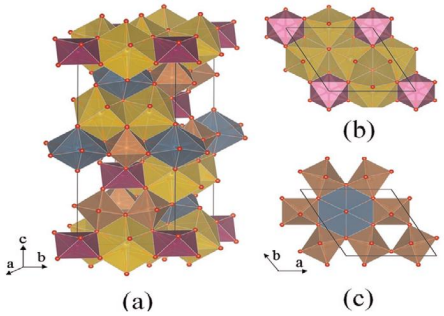

Crystal structure of rhombohedral pyrochlore $Mn_2Ln_3Sb_3O_{14}$ (Ln=La, Pr, and Nd) showing the staking of Ln_3Mn and $MnSb_3$ layers (a). (b) and (c) show the connections between $Mn1O_6$ and LnO_8 and between $Mn2O_8$ and SbO_6 polyhedra, respectively.

Electron density distribution and disordered crystal structure of 8*H*-SiAlON, $Si_{3-x}Al_{1+x}O_xN_{5-x}$ (x~2.2)
Hiroki Banno, Toru Asaka and Koichiro Fukuda
page 169

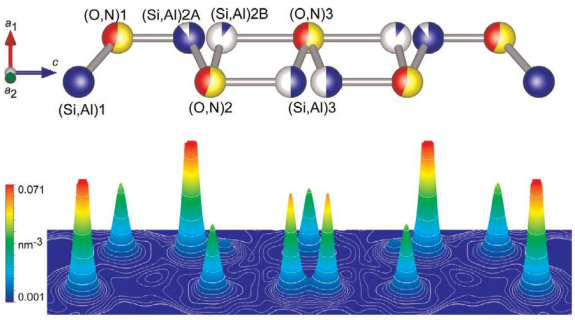

Bird's eye view of electron densities up to 49.3% (0.071 nm^{-3}) of the maximum on the plane parallel to (110) with the corresponding atomic arrangements of $Si_{0.8}Al_{3.2}O_{2.2}N_{2.8}$.

Tailoring surface properties and structure of layered double hydroxides using silanes with different number of functional groups
Qi Tao, Hongping He, Tian Li, Ray L. Frost, Dan Zhang and Zisen He
page 176

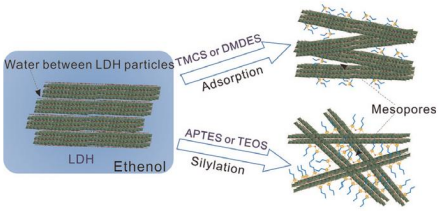

The replacement of water by ethanol in the tactoids and aggregations of LDHs, and the polysiloxane oligomers formed during silylation process can dramatically increase the BET surface area (S_{BET}) and the total pore volume (V_p) of the silylated products.

Crystal structures of orthorhombic, hexagonal, and cubic compounds of the $Sm_{(x)}Yb_{(2-x)}TiO_5$ series
Robert D. Aughterson, Gregory R. Lumpkin, Massey de los Reyes, Neeraj Sharma, Christopher D. Ling, Baptiste Gault, Katherine L. Smith, Maxim Avdeev and Julie M. Cairney
page 182

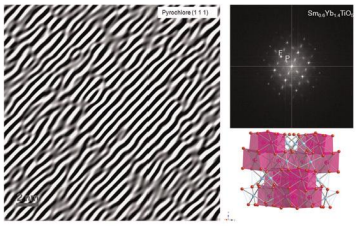

A high resolution image of the compound $Sm_{0.6}Yb_{1.4}TiO_5$ showing contrast from lattice fringes and the corresponding fast Fourier transform (FFT) of the HREM image with pyrochlore related diffraction spots marked "P" and fluorite marked "F". The crystal is oriented down the [1 1 0] zone axis based on the *Fd*-3*m* structure. The ideal crystal structure (no vacancies) of the cubic, pyrochlore-like ($Sm_{0.6}Yb_{1.4}TiO_5$).

Porous Co_3O_4 nanorods as anode for lithium-ion battery with excellent electrochemical performance
Jinxue Guo, Lei Chen, Xiao Zhang and Haoxin Chen
page 193

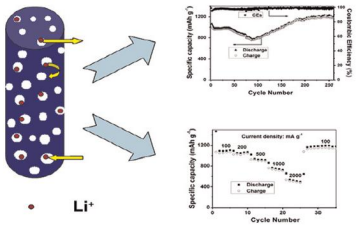

1D porous Co_3O_4 nanostructure as anode for lithium-ion battery with excellent electrochemical performance.

Continued

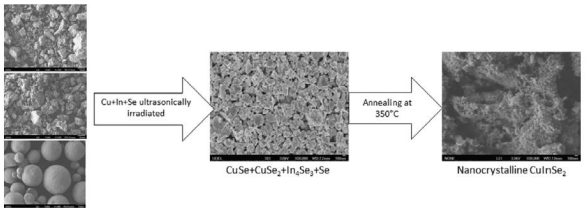

Ultrasonically irradiation and thermally annealing of Cu+In+Se mixture result in nanocrystalline $CuInSe_2$ particles due to the proposed reaction pathways.

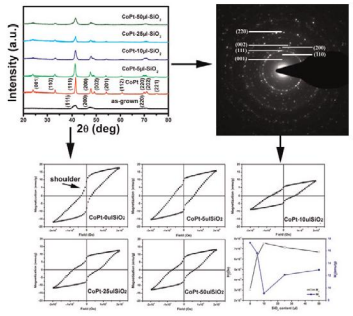

$L1_0$ CoPt alloy nanoparticles with various contents of SiO_2 are synthesized by sol–gel method. The effects of SiO_2 on the structure and magnetic properties of CoPt nanoparticles are investigated.

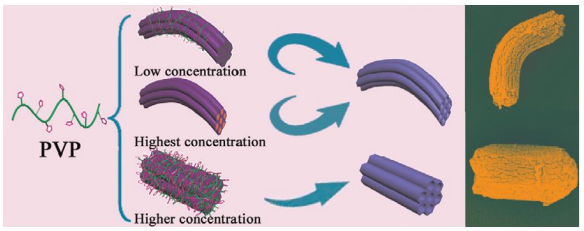

Curved rod-shaped mesoporous silica can be obtained at low and the highest PVP concentration, while straight rod-shaped mesoporous silica can be obtained at higher PVP concentration.

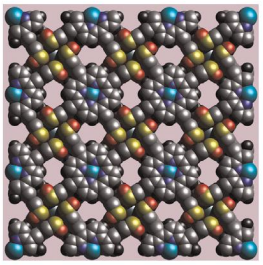

A terbium–zinc porphyrin $[TbZn(TPPS)H_3O]_n$ has been obtained from a solvothermal reaction. It features a condensed 3-D porous open framework. It shows good thermal stability.

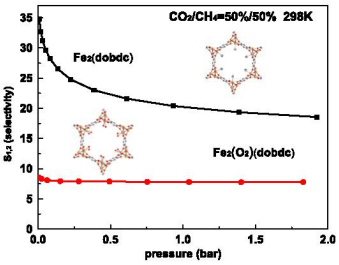

The selectivity of CO_2/CH_4 mixture (50%/50%) on $Fe_2(dobdc)$ and $Fe_2(O_2)(dobdc)$.

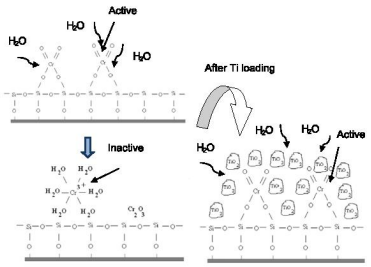

The load of Ti on the Cr modified MCM-41 produces a TiO_2 cover that protects the active Cr species from their reduction by the environmental humidity.

In-situ and self-distributed: A new understanding on catalyzed thermal decomposition process of ammonium perchlorate over Nd_2O_3

Min Zou, Xin Wang, Xiaohong Jiang and Lude Lu

page 235

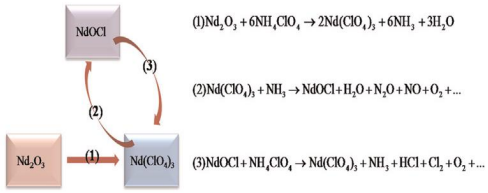

In-situ and self-distributed reaction process in thermal decomposition of AP catalyzed by Nd_2O_3.

Fabrication of p-type porous silicon nanowire with oxidized silicon substrate through one-step MACE

Shaoyuan Li, Wenhui Ma, Yang Zhou, Xiuhua Chen, Yongyin Xiao, Mingyu Ma, Feng Wei and Xi Yang

page 242

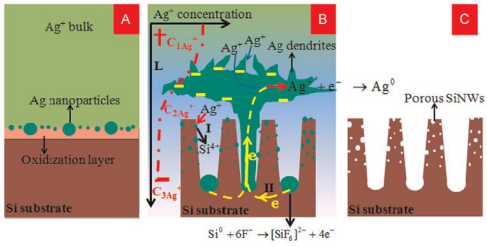

Schematic cross-sectional views of PSiNWs array formation by etching oxidized silicon wafer in HF/$AgNO_3$ solution. (A) At the starting point; (B) during the etching process; and (C) after Ag dendrites remove.

Preparation of acid-base bifunctional mesoporous KIT-6 (KIT: Korea Advanced Institute of Science and Technology) and its catalytic performance in Knoevenagel reaction

Ling Xu, Chunhua Wang and Jingqi Guan

page 250

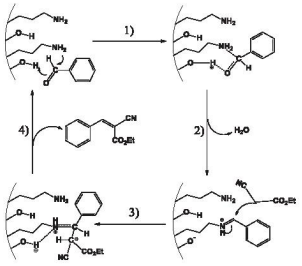

The postulated steps of mechanism for the acid-base catalyzed process are as follows: (1) the aldehyde gets activated by the surface acidic sites which allow the amine undergoes nucleophilic to attack the carbonyl carbon of benzaldehyde. (2) Water is released in the formation of imine intermediate. (3) The ethyl cyanoacetate reacts with the intermediate. (4) The benzylidene ethyl cyanoacetate is formed and the amine is regenerated.

Assembling supramolecular networks by halogen bonding in coordination polymers driven by 5-bromonicotinic acid

Jin-Zhong Gu, Jiang Wu, Alexander M. Kirillov, Dong-Yu Lv, Yu Tang and Jin-Cai Wu

page 256

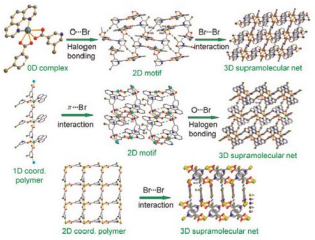

Six coordination compounds driven by 5-bromonicotinic acid have been generated and structurally characterized, revealing diverse metal-organic networks that are further reinforced and extended via various halogen bonding interactions.

Structural, electrochemical and magnetic characterization of the layered-type $PrBa_{0.5}Sr_{0.5}Co_2O_{5+\delta}$ perovskite

Abul K. Azad, Jung H. Kim and John T.S. Irvine

page 268

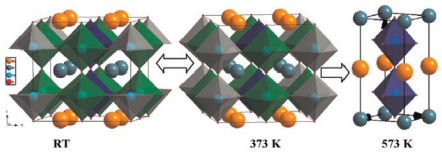

Structural phase changes in $PrBa_{0.5}Sr_{0.5}Co_2O_{5+\delta}$ at elevated temperatures determined by neutron powder diffraction. Depending on oxygen occupancy it form different phases at different temperatures. This pictures show the schematic 3D diagram of $PrBa_{0.5}Sr_{0.5}Co_2O_{5+\delta}$ at 295 K (a), 373 K (b) and 573 K (c). Co atoms are inside the octahedra/pyramid. Ba and Sr occupy the same site. Oxygens are in the corner of polyhedra.

Three series of quaternary rare-earth transition-metal pnictides with $CaAl_2Si_2$-type structures: *RE*$CuZnAs_2$, *RE*$AgZnP_2$, and *RE*$AgZnAs_2$

Stanislav S. Stoyko, Krishna K. Ramachandran, Peter E.R. Blanchard, Kimberly A. Rosmus, Jennifer A. Aitken and Arthur Mar

page 275

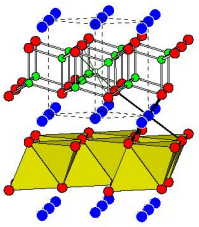

Cu or Ag atoms are disordered with Zn atoms over the tetrahedral site within relatively rigid $[M_2Pn_2]$ slabs in three series of quaternary pnictides adopting the $CaAl_2Si_2$-type structure.

Continued

Chemical compatibility study of melilite-type gallate solid electrolyte with different cathode materials
Alessandro Mancini, Valeria Felice, Isabella Natali Sora, Lorenzo Malavasi and Cristina Tealdi
page 287

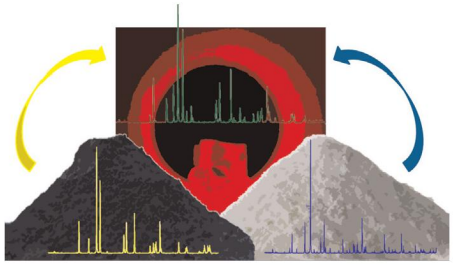

Chemical reactivity between cathodes and electrolytes is a crucial issue for long term SOFCs stability and performances. In this study, chemical reactivity between selected cathodic materials and the ionic conducting melilite $La_{1.50}Sr_{0.50}Ga_3O_{7.25}$ has been extensively investigated by means of X-ray powder diffraction.

Structural and electronic properties of $Sr_{1-x}Ca_xTi_{0.5}Mn_{0.5}O_3$
Ilyas Qasim, Peter E.R. Blanchard, Brendan J. Kennedy, Takashi Kamiyama, Ping Miao and Shuki Torii
page 293

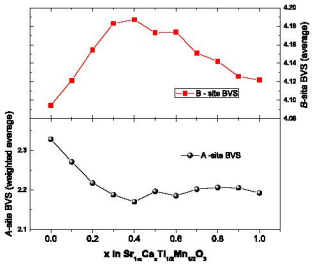

Changes in the bond valence sums for the *A*- and *B*-sites in $Sr_{1-x}Ca_xMn_{0.5}Ti_{0.5}O_3$ reflect changes in the symmetry of the oxides.

Rapid Communications

Structural distortion and band gap opening of hard MnB_4 in comparison with CrB_4 and FeB_4
Meng Yang, Yachun Wang, Jinlei Yao, Zhiping Li, Jian Zhang, Lailei Wu, Hui Li, Jingwu Zhang and Huiyang Gou
page 52

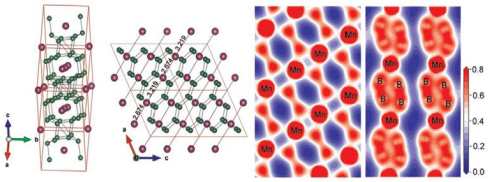

$P2_1/c$-type structure for MnB_4 characterizes rhomboid-B_4 units and alternately short and long Mn–Mn chains.

Language services. Authors who require information about language editing and copyediting services pre- and post-submission please visit http://www.elsevier.com/locate/languagepolishing or our customer support site at http://epsupport.elsevier.com. Please note Elsevier neither endorses nor takes responsibility for any products, goods or services offered by outside vendors through our services or in any advertising. For more information please refer to our Terms & Conditions http://www.elsevier.com/termsandconditions

For a full and complete Guide for Authors, please go to: http://www.elsevier.com/locate/jssc

Journal of Solid State Chemistry has no page charges.